Engineered Unique Elastic Modes at a $BaTiO_3/(2\times1)$-Ge(001) Interface

D. P. Kumah,[1,*] M. Dogan,[1] J. H. Ngai,[1] D. Qiu,[1] Z. Zhang,[2] D. Su,[3] E. D. Specht,[4] S. Ismail-Beigi,[1] C. H. Ahn,[1] and F. J. Walker[1,*]

[1]*Center for Research on Interface Structures and Phenomena, Yale University, New Haven, Connecticut 06520, USA*
[2]*Argonne National Laboratory, Advanced Photon Source, Argonne, Illinois 60439, USA*
[3]*Brookhaven National Laboratory, Center for Functional Nanomaterials, Upton, New York 11973, USA*
[4]*Oak Ridge National Laboratory, Oak Ridge, Tennessee 37831, USA*

(Received 5 August 2015; revised manuscript received 22 October 2015; published 7 March 2016)

The strong interaction at an interface between a substrate and thin film leads to epitaxy and provides a means of inducing structural changes in the epitaxial film. These induced material phases often exhibit technologically relevant electronic, magnetic, and functional properties. The 2×1 surface of a Ge(001) substrate applies a unique type of epitaxial constraint on thin films of the perovskite oxide $BaTiO_3$ where a change in bonding and symmetry at the interface leads to a non-bulk-like crystal structure of the $BaTiO_3$. While the complex crystal structure is predicted using first-principles theory, it is further shown that the details of the structure are a consequence of hidden phases found in the bulk elastic response of the $BaTiO_3$ induced by the symmetry of forces exerted by the germanium substrate.

DOI: 10.1103/PhysRevLett.116.106101

Strain coupling in perovskite-perovskite systems has led to the control and enhancement of a wide range of physical properties including metal-insulator transitions in the rare-earth nickelates [1–4], ferroelectricity and ferromagnetism in the titanates [5–7], and improper ferroelectricity in titanate multilayers [8]. Epitaxial constraints are particularly important in controlling the physical properties of most perovskite transition metal oxides whose properties are strongly coupled to local and long-range structural distortions of the oxygen octahedral sublattice [9,10]. These properties can be continuously tuned by modifying the amplitudes of the lattice distortions. However, by coupling to more complex interfacial degrees of freedom that go beyond simple elastic strain, electronic and magnetic effects can potentially be coupled in order to give rise to multiferroic effects and complex orderings of electronic charge and spin [11–13]. Recent advances in the epitaxial growth of perovskite oxides on semiconductors such as Si [14–17], Ge [18–20], and GaAs [21–23] allow for structural coupling to even more complex symmetry degrees of freedom that are not accessible in standard perovskite-perovskite epitaxy [24]. Separately, in a more technological vein, the growth compatibility of complex oxides with semiconductors has allowed the monolithic integration of the functional properties of oxides with well-established complementary metal-oxide-semiconductor technologies [25].

In this Letter, we demonstrate the design of a nonbulk structural phase of the transition metal ferroelectric $BaTiO_3$ (BTO) using an interfacial structural motif that strongly couples to symmetry-lowering structural distortions in the BTO. Bulk BTO has a tetragonal $P4mm$ structure at room temperature with an in-plane lattice constant of 3.99 Å and a ferroelectric polar distortion along its c axis [26]. We report on lattice distortions in thin BTO films grown on the reconstructed Ge(001) surface with a lower Pm planar symmetry arising from asymmetric Ge surface dimer rows [27,28]. The net result is a strong interfacial coupling to in-plane symmetry-breaking distortions in the BTO that stabilize a nonbulk and distorted BTO interfacial phase. The nonbulk features of this structure include breathing-mode distortions of the oxygen octahedra and cation rumpling. This phase leads to an in-plane component of the polarization in the BTO in addition to significant oxygen octahedral distortions: in other complex transition metal perovskite oxide systems, such distortions are associated with charge, spin, and orbital ordering [29–31]. While the in-plane polarization can be related to the room-temperature stabilization of the bulk low-temperature orthorhombic BTO phase, the period-doubling octahedral distortions that we observe are unique to the BTO/Ge interface and are associated with stiff bulk modes that are stabilized by the forces exerted by the reconstructed Ge surface. Using a combination of synchrotron x-ray diffraction, transmission electron microscopy, and density functional theory calculations, we show that the observed distortions can be parametrized by considering the lattice distortion modes excited by the symmetry of the imposed epitaxial constraint.

Thin films of BTO with thicknesses of 2.5 and 5.5 unit cell (uc) are grown on single crystalline Ge(001) substrates using reactive molecular beam epitaxy [17,19,32–34]. A 0.5 monolayer of Ba is deposited at 440 °C on the Ge surface to passivate the surface and prevent the oxidation of the Ge surface. The wafer is then cooled to room temperature where an additional 0.5 monolayer of Ba is deposited, followed by codeposition of two monolayers each of BaO

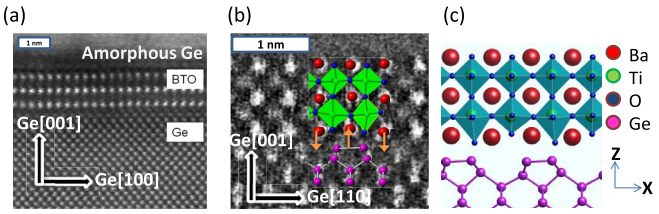

FIG. 1. (a) High angle annular dark field image of 2.5-uc BTO/Ge along the Ge[100] zone axis. (b) Superimposed on the TEM image taken along the Ge[110] zone axis is a model structure of the system determined from surface x-ray diffraction measurements. The red arrows indicate the rumpling of the interfacial Ba along the [001] axis. (c) DFT-predicted ground-state structure of the 2.5-uc BTO/Ge system.

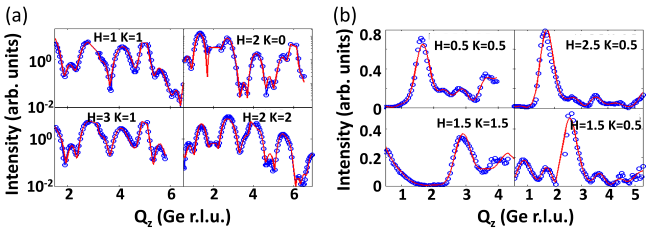

FIG. 2. (a) Integer-order (logarithmic vertical scale) and (b) superstructure (linear vertical scale) crystal truncation rods measured (blue circles) for a 2.5-uc BTO film grown on Ge(001) using molecular beam epitaxy. The model structure of the BTO/Ge interface shown in Fig. 1(b) is derived from the fits (red lines) to the measured data.

and TiO_2. The low-temperature deposition leads to the formation of amorphous BTO as evidenced by a diffuse RHEED pattern. The wafer is then heated to 500 °C in UHV whence the amorphous BaO and TiO_2 react to form crystalline $BaTiO_3$. To create the 5.5-uc sample, three additional monolayers of BaO and TiO_2 are codeposited at a substrate temperature of 570 °C. We note that the higher-temperature deposition of the three additional layers for the 5.5-uc sample may lead to changes in the stoichiometry and interfacial structure as discussed below. Finally, for the 2.5-uc sample, a 7-nm-thick capping layer of amorphous Ge is deposited at room temperature to protect the ultrathin $BaTiO_3$ film.

To characterize the structure of the BTO films, transmission electron microscopy measurements are carried out at Brookhaven National Laboratory. Figures 1(a) and 1(b) show high angle annular dark field images obtained along Ge[110] and Ge[100] zone axes, respectively, for the 2.5-uc BTO/Ge sample. The images indicate an abrupt interface with coherent atomic registry between the BTO film and the Ge. As explained below, the reduced contrast for the interfacial Ge layer is attributed to a Ge reconstruction and not to structural disorder in agreement with Fredrickson *et al.* where the interface is prepared starting with a Zintl phase consisting of half a ML of Sr on Ge(001) [20].

To confirm the ordered nature of the interface and the effect of the coupling across the interface, we use synchrotron x-ray diffraction measurements to determine the atomic structure of the system: atomic-scale structure of the samples are determined from the analysis of crystal truncation rods (CTRs) [35]. In addition to integer-order rods observed for both the 2.5- and 5.5-uc samples, for the 2.5-uc sample, superstructure reflections consistent with a 2×1 symmetry with respect to the bulk Ge are observed. From the periodicity of the superstructure reflections in the direction in reciprocal space perpendicular to the film-substrate interface, the 2×1 symmetry is determined to extend from the interface into the BTO film.

Atomic positions are derived from the measured CTRs and superstructure reflections by fitting using a chi-square minimization genetic fitting algorithm program, GenX [36]. For this analysis, we consider the coherent average of two 90° rotational domains that arise due to atomic layer steps on the Ge(001) surface. Figures 2(a) and 2(b) show measured diffraction intensities along integer and half-order rods, respectively, and their associated fits for the converged 2.5-uc sample. The XRD-determined structure of the 2.5-uc sample is shown superimposed on the TEM image of the same sample in Fig. 1(b). The main features of the XRD structure are well reproduced in the TEM image: i.e., the rumpling of a full monolayer of Ba at the interface and the displacement of Ti along the BTO [100] direction. The O positions, which are not resolved in the TEM image, are determined from the x-ray CTR analysis.

For the 2.5-uc sample, the interfacial Ge atoms are displaced in plane from their bulk positions forming dimer rows along the [010] direction. A monolayer of BaO is in direct contact with the topmost Ge layer. Rumpling of the interfacial BaO occurs in response to the Ge interface dimerization doubling the size of the BTO unit cell in the [100] direction. The BaO displacements couple to displacements of the Ti and O ions resulting in distortion of the entire film relative to the expected tetragonal structure. Along [100], the alternate contraction and expansion of the TiO_6 octahedra is consistent with a breathing-mode distortion, absent in the bulk phase diagram of BTO. The distortions are observed to decay in the direction of the film growth.

The stability of the observed structure for the 2.5-uc sample is confirmed from first-principles density functional theory (DFT) calculations (see the Supplemental Material [37] for full details). The ground-state relaxed atomic coordinates of the BTO/Ge system are determined theoretically and are found to be in agreement with the experimentally measured structure [Fig. 1(c)].

In contrast to the 2.5-uc film, for the thicker 5.5-uc sample the CTR analysis and the absence of superstructure Bragg reflections show that the entire system of BTO and interfacial Ge have a 1×1 symmetry. The 5.5-uc BTO film has lattice constants $a = b = 3.99$ Å and $c = 4.12$ Å in agreement with those of bulk tetragonal BTO. Fits to the

CTRs for the 5.5-uc film are shown in the Supplemental Material [37]. This points to a link explored below between the growth procedure for the thicker film and the manifestation or suppression of the interfacial distortions in the BTO.

Recent results show that a diverse range of interface structures can be stabilized for interfaces with varying cation and oxygen stoichiometry. BTO films grown with a higher alkaline earth metal content show that the Ge dimers are stable, even for thicker films, using a ½-ML Sr Zintl template layer on Ge [20]. In addition, prior theoretical calculations on the similar $SrTiO_3/Si$ interface indicate a strong dependence of the dimerization of the interfacial semiconductor layer on both the cation and oxygen stoichiometry, where low oxygen concentrations at the $SrTiO_3/Si$ interface destabilize the Si dimers resulting in a 1×1 interface [43]. We have performed systematic theoretical calculations (see the Supplemental Material [37] for full details) to clarify the effects of oxygen stoichiometry and film thickness on the relative stabilities of 1×1 and 2×1 BTO/Ge interface structures. In brief, oxygen deficiency stabilizes the 1×1 interfacial structure: this is linked to electron doping of the interface (due to oxygen vacancy formation) and concomitant weakening of Ge-Ge dimers caused by electron occupation of antibonding states of the dimerized Ge layer. This observation means that experimentally controlling the interfacial oxygen stoichiometry at oxide-semiconductor interfaces can stabilize functional structural distortions.

To understand the BTO structural response for the 2.5-uc-thick films, we consider the lattice modes associated with bulk BTO [44]. The elastic response of atom l of the BTO lattice to a force $F_{l\alpha}$ is given by $F_{l\alpha} = -\sum_{l'\beta} K_{l\alpha,l'\beta}\, u_{l'\beta}$, where $K_{l\alpha,l'\beta}$ is the interatomic force constant matrix connecting the force along Cartesian direction α on atom l to the displacement $u_{l'\beta}$ of atom l' in direction β. The interatomic force constants are calculated for a reference bulk phase of BTO using *ab initio* density functional perturbation theory calculations [45]. We then diagonalize the force constant matrix to obtain a set of static normal modes or eigenmodes. By projecting the computed BTO lattice distortions in the heterostructure (relative to the undistorted bulk BTO reference structure) onto these static eigenmodes, the distortions are described in the basis of eigenmodes of the bulk force constant matrix that immediately identifies unstable versus stiff modes. We have performed this analysis using the eigenmodes of the cubic high-symmetry phase of bulk BTO. We choose this reference phase for simplicity. We have explicitly verified that other choices of reference (e.g., tetragonal phase or strained bulk phases) yield similar results: the largest projections are always onto the soft modes at zero wave vector.

Figure 3 shows eigenmode dispersion curves along high-symmetry directions in reciprocal space for BTO in its high-symmetry cubic perovskite structure. An $8 \times 8 \times 8$ q-point mesh is used to sample the Brillouin zone. Intermediate q points are determined by Fourier interpolation. Modes with imaginary eigenvalues are soft or unstable. The circles in Fig. 3 indicate the magnitude of the projections of the atomic displacements in the 2.5-uc-thick BTO slab onto the eigenmodes. Displacement patterns and projections are calculated for each 1-uc-thick BTO that can be extracted from the BTO slab. Figure 3(a) shows the projections for the two atomic layers (BaO and TiO_2), which form the first BTO uc adjacent to the interface. Each atom is distorted away from a reference

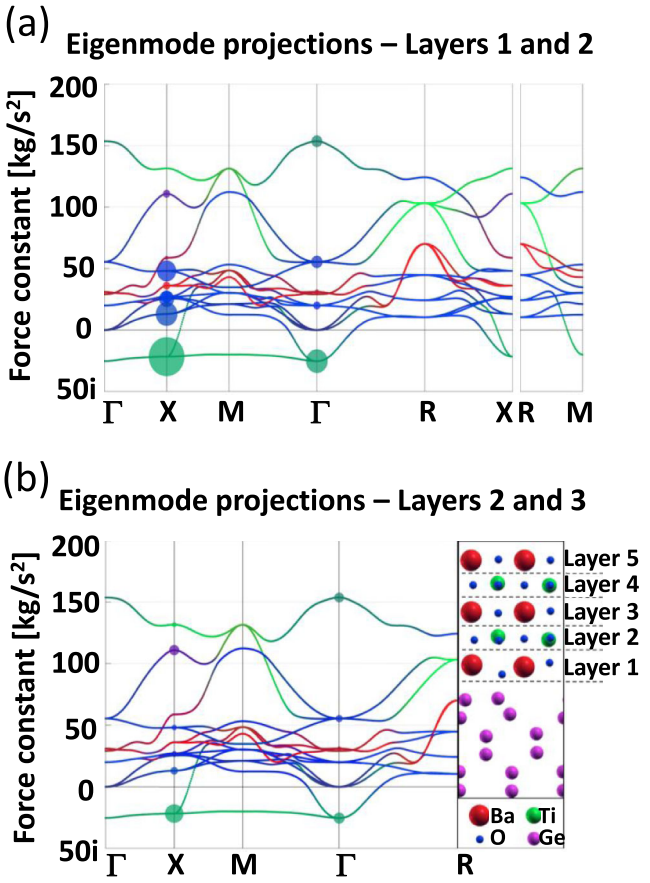

FIG. 3. Force constant matrix eigenmode dispersion curves in reciprocal space for bulk cubic $BaTiO_3$. The colors correspond to the atomic content of each mode: red, green, blue correspond to amplitudes of motion of Ba, Ti, O atoms, respectively, following Ghosez *et al.* [44]. Solid circles superimposed on the dispersion curves express the decomposition of atomic displacements at the interface onto modes with Γ and X symmetry. The radii of the circles are proportional to the magnitude of the projections of the atomic displacements in the 2.5-uc-thick BTO slab onto the eigenmodes. (a) The projections of the displacements of the first BaO and TiO_2 layers adjacent to the interface. (b) The projections for the first TiO_2 layer and the second BaO layer above it. The theoretical ground state of the BTO/Ge system is reproduced in the inset with the numbering of the atomic layers and the color-coding of the atom types.

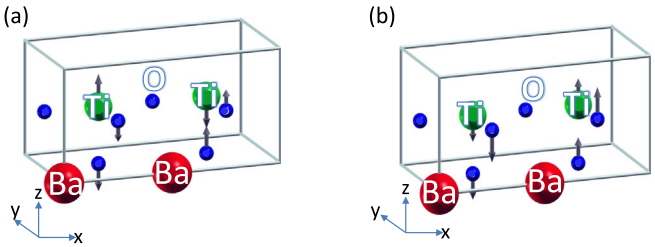

FIG. 4. (a) Atomic motions for force constant matrix eigenmode contributing the most to the displacements of the 2.5-uc-thick BTO slab. The mode is soft at the X point so that it involves antiparallel displacements of planar O and Ti. (b) Lowest energy stiff acoustic mode at X where the Ti and O atoms move in the same direction.

configuration given by a pair of strained cubic cells (joined in the x direction to make a $2 \times 1 \times 1$ cell) in which the atoms are at the high-symmetry locations of the perovskite structure. The geometric center of this reference cell is determined such that it coincides with the center of the atomic positions in the particular $2 \times 1 \times 1$ cell that is taken from the BTO film. This choice for the center makes the projections onto the acoustic modes at Γ vanish. (For more information regarding the choice of reference cell, see the Supplemental Material [37].) We decompose the displacements in a $2 \times 1 \times 1$ cell into the displacement modes obtained from a $1 \times 1 \times 1$ cell, which corresponds to the modes at the Γ and the X points of the $1 \times 1 \times 1$ cell (30 projections in total). Figure 3(b) shows the projections for the next 1-uc-thick subset of the slab. Away from the interface, the projections reduce in amplitude, but the dominant modes remain the same. As expected, the unstable modes with displacements normal to the interfacial plane account for most of the observed structural distortions. In Fig. 4, the two leading eigenmodes [two largest circles at the X point in Fig. 3(a)] for the interfacial BTO are shown. Figure 4(a) shows the most dominant displacement mode that involves out-of-plane O and Ti motion, where the Ti atoms move in the opposite direction as the O atoms that are on the same (011) plane. Shown in Fig. 4(b) is a stiff acoustic mode, which is the next leading mode where the Ti atoms move in the same direction as the O atoms.

A significant part of the lattice distortion involves zone center distortions about the Γ point that result in nonzero polarization in the x and z directions, which corresponds to the bulk orthorhombic phase stable between 183 and 278 K (see the Supplemental Material [37] for discussion of projections of BTO bulk orthorhombic displacements). The ionic polarization $\vec{P}$ of the interfacial layer of the 2.5-uc film is determined from the summation $\vec{P} = (e/\Omega)\sum_i Z_i^* x_i$ where Z_i^* and x_i are the Born effective charges computed for a reference strained cubic bulk BTO, as discussed above, and the displacements from the reference position of the ith ion, respectively. Ω is the volume of the $2 \times 1 \times 1$ uc over which the summation is carried out. The spontaneous ionic polarization of the first interfacial BTO uc is estimated to be 54 μC/cm^2 along the BTO $\{101\}$ axis, which is comparable to the bulk polarization for orthorhombic BTO of 36 μC/cm^2 [46]. The large value may be a consequence of strain imposed by the Ge substrate. The lattice parameter of Ge (3.99 Å) is smaller than the a and b parameter of o-$BaTiO_3$ and larger than the c axis of o-$BaTiO_3$, increasing the orthorhombic distortion and the larger observed polarization. We note that since an equivalent BTO structure is obtained by applying a reflection operation to the system through the yz plane, the in-plane component of the polarization does not have a preferred direction and, hence, in principle, may be switched. In practice, however, the computed energy barrier (using the nudged elastic bands method [47]) of 0.6 eV per 2×1 cell is on the large side.

In summary, we have shown how the symmetry of an epitaxial constraint can induce a phase of $BaTiO_3$ not found in the bulk. The structure of this phase is a seemingly complex distortion of the perovskite structure at an interface that is accurately calculated by applying first-principles theory to a many-atom model of the interface. We have reduced this complexity by showing that many of the structural details of the specific structure are encoded in the bulk force constant matrix of $BaTiO_3$ and expressed when coupled to the 2×1 symmetry of the Ge substrate. This observation suggests an approach to design materials properties by using a catalog of force constant matrices to identify materials with specific structural motifs. Substrates with symmetries that couple to soft modes of the material can then be chosen that enhance these motifs. For example, replacing the B-site Ti ions with other transition ions such as Mn and Ni, where breathing-mode distortions are associated with charge ordering, it is likely that interfacial structural distortions similar to those measured here for BTO on Ge will lead to charge "stripes," metal-insulator transitions, or enhanced coupling with ferroelectric polarization.

The authors acknowledge support from the NSF under Grants No. MRSEC DMR-1119826 (CRISP) and No. DMR-1309868. Work at the Advanced Photon Source was supported by the DOE, Office of Science, Office of Basic Energy Sciences, under Contract No. DE-AC02-06CH11357. Work at Brookhaven was supported by the U.S. Department of Energy, Office of Basic Energy Science, under Contract No. DE-AC02-98CH10886. Computational facilities are supported by NSF Grant No. CNS 08-21132 and by the facilities and staff of the Yale University Faculty of Arts and Sciences High Performance Computing Center. Additional computations are carried out via the NSF TeraGrid and XSEDE resources through Grant No. TG-MCA08X007.

*Corresponding authors.
dpkumah@ncsu.edu, fred.walker@yale.edu

[1] E. J. Moon, J. M. Rondinelli, N. Prasai, B. A. Gray, M. Kareev, J. Chakhalian, and J. L. Cohn, Strain-controlled band engineering and self-doping in ultrathin $LaNiO_3$ films, Phys. Rev. B **85**, 121106 (2012).

[2] J. M. Rondinelli, S. J. May, and J. W. Freeland, Control of octahedral connectivity in perovskite oxide heterostructures: An emerging route to multifunctional materials discovery, MRS Bull. **37**, 261 (2012).

[3] M. K. Stewart, J. Liu, M. Kareev, J. Chakhalian, and D. N. Basov, Mott physics near the insulator-to-metal transition in $NdNiO_3$, Phys. Rev. Lett. **107**, 176401 (2011).

[4] S. J. May, C. R. Smith, J. W. Kim, E. Karapetrova, A. Bhattacharya, and P. J. Ryan, Control of octahedral rotations in $(LaNiO_3)n/(SrMnO_3)m$ superlattices, Phys. Rev. B **83**, 153411 (2011).

[5] J. H. Lee *et al.*, A strong ferroelectric ferromagnet created by means of spin-lattice coupling, Nature (London) **466**, 954 (2010).

[6] C. Ederer and N. A. Spaldin, Effect of Epitaxial Strain on the Spontaneous Polarization of Thin Film Ferroelectrics, Phys. Rev. Lett. **95**, 257601 (2005).

[7] D. G. Schlom, L.-Q. Chen, C.-B. Eom, K. M. Rabe, S. K. Streiffer, and J.-M. Triscone, Strain tuning of ferroelectric thin films, Annu. Rev. Mater. Res. **37**, 589 (2007).

[8] E. Bousquet, M. Dawber, N. Stucki, C. Lichtensteiger, P. Hermet, S. Gariglio, J.-M. Triscone, and P. Ghosez, Improper ferroelectricity in perovskite oxide artificial superlattices, Nature (London) **452**, 732 (2008).

[9] J. W. Reiner, F. J. Walker, and C. H. Ahn, Atomically Engineered Oxide Interface, Science **323**, 1018 (2009).

[10] P. Zubko, S. Gariglio, M. Gabay, P. Ghosez, and J.-M. Triscone, Interface Physics in Complex Oxide Heterostructures, Annu. Rev. Condens. Matter Phys. **2**, 141 (2011).

[11] N. A. Spaldin and M. Fiebig, The renaissance of magnetoelectric multiferroics, Science **309**, 391 (2005).

[12] N. A. Benedek and C. J. Fennie, Hybrid Improper Ferroelectricity: A Mechanism for Controllable Polarization-Magnetization Coupling, Phys. Rev. Lett. **106**, 107204 (2011).

[13] J. M. Tranquada, J. D. Axe, N. Ichikawa, A. R. Moodenbaugh, Y. Nakamura, and S. Uchida, Coexistence of, and competition between, superconductivity and charge-stripe order in $La_{1.6-x}Nd_{0.4}SrxCuO_4$, Phys. Rev. Lett. **78**, 338 (1997).

[14] Y. Segal, J. W. Reiner, A. M. Kolpak, Z. Zhang, S. Ismail-Beigi, C. H. Ahn, and F. J. Walker, Atomic Structure of the Epitaxial $BaO/Si(001)$ Interface, Phys. Rev. Lett. **102**, 116101 (2009).

[15] M. B. Nardelli, F. J. Walker, and R. A. McKee, Crystalline oxides on semiconductors: a future for the nanotransistor, Phys. Status Solidi B **241**, 2279 (2004).

[16] A. Lin, X. Hong, V. Wood, A. A. Verevkin, C. H. Ahn, R. A. McKee, F. J. Walker, and E. D. Specht, Epitaxial growth of $Pb(Zr_{0.2}Ti_{0.8})O_3$ on Si and its nanoscale piezoelectric properties, Appl. Phys. Lett. **78**, 2034 (2001).

[17] R. A. McKee, F. J. Walker, and M. F. Chisholm, Crystalline oxides on silicon: The first five monolayers, Phys. Rev. Lett. **81**, 3014 (1998).

[18] M. Hudait, Y. Zhu, N. Jain, D. Maurya, Y. Zhou, and S. Priya, Quasi-zero lattice mismatch and band alignment of $BaTiO_3$ on epitaxial (110) Ge, J. Appl. Phys. **114**, 024303 (2013).

[19] C. Merckling, G. Saint-Girons, C. Botella, G. Hollinger, M. Heyns, J. Dekoster, and M. Caymax, Molecular beam epitaxial growth of $BaTiO_3$ single crystal on Ge-on-Si (001) substrates, Appl. Phys. Lett. **98**, 092901 (2011).

[20] K. D. Fredrickson, P. Ponath, A. B. Posadas, M. R. McCartney, T. Aoki, D. J. Smith, and A. A. Demkov, Atomic and electronic structure of the ferroelectric $BaTiO_3/Ge(001)$ interface, Appl. Phys. Lett. **104**, 242908 (2014).

[21] Y. Liang *et al.*, *MRS Proceedings* (Cambridge University Press, Cambridge, England, 2003), p. E8.4.

[22] Y. Liang, J. Kulik, T. C. Eschrich, R. Droopad, Z. Yu, and P. Maniar, Hetero-epitaxy of perovskite oxides on $GaAs(001)$ by molecular beam epitaxy, Appl. Phys. Lett. **85**, 1217 (2004).

[23] R. Klie, Y. Zhu, E. I. Altman, and Y. Liang, Atomic structure of epitaxial $SrTiO_3 - GaAs(001)$ heterojunctions, Appl. Phys. Lett. **87**, 143106 (2005).

[24] J. L. Wang, A. Pancotti, P. Jegou, G. Niu, B. Gautier, Y. Y. Mi, L. Tortech, S. Yin, B. Vilquin, and N. Barrett, Ferroelectricity in a quasiamorphous ultrathin $BaTiO_3$ film, Phys. Rev. B **84**, 205426 (2011).

[25] A. A. Demkov and A. B. Posadas, *Integration of Functional Oxides with Semiconductors* (Springer, New York, 2014), p. 159.

[26] G. Shirane, H. Danner, and R. Pepinsky, Neutron diffraction study of orthorhombic $BaTiO_3$, Phys. Rev. **105**, 856 (1957).

[27] H. J. W. Zandvliet, The $Ge(001)$ surface, Phys. Rep. **388**, 1 (2003).

[28] P. Kruger and J. Pollmann, Dimer reconstruction of diamond(001), $Si(001)$ and $Ge(001)$ surfaces, Phys. Rev. Lett. **74**, 1155 (1995).

[29] B. J. Sternlieb, J. P. Hill, U. C. Wildgruber, G. M. Luke, B. Nachumi, Y. Moritomo, and Y. Tokura, Charge and magnetic order in $La_{0.5}Sr_{1.5}MnO_4$, Phys. Rev. Lett. **76**, 2169 (1996).

[30] D. Reznik, L. Pintschovius, M. Ito, S. Iikubo, M. Sato, H. Goka, M. Fujita, K. Yamada, G. D. Gu, and J. M. Tranquada, Tranquada, Electron-phonon coupling reflecting dynamic charge inhomogeneity in copper oxide superconductors, Nature (London) **440**, 1170 (2006).

[31] A. Cammarata and J. M. Rondinelli, Octahedral engineering of orbital polarizations in charge transfer oxides, Phys. Rev. B **87**, 155135 (2013).

[32] R. Droopad, J. Wang, K. Eisenbeiser, Z. Yu, J. Ramdani, J. A. Curless, C. D. Overgaard, J. M. Finder, J. A. Hallmark, V. Kaushik, B. Y. Nguyen, D. S. Marshall, and W. J. Ooms, Epitaxial Oxide Films on Silicon: Growth, Modeling and Device Properties, in *MRS Proceedings* (Cambridge University Press, Cambridge, England, 2000), Vol. 619, p. 155.

[33] J. W. Reiner, A. M. Kolpak, Y. Segal, K. F. Garrity, S. Ismail-Beigi, C. H. Ahn, and F. J. Walker, Crystalline Oxides on Silicon, Adv. Mater. **22**, 2919 (2010).

[34] S.-H. Baek and C.-B. Eom, Epitaxial integration of perovskite-based multifunctional oxides on silicon, Acta Mater. **61**, 2734 (2013).

[35] D. P. Kumah *et al.*, The atomic structure and polarization of strained $SrTiO_3$/Si, Appl. Phys. Lett. **97**, 251902 (2010).
[36] M. Bjorck and G. Andersson, GenX: an extensible X-ray reflectivity refinement program utilizing differential evolution, J. Appl. Crystallogr. **40**, 1174 (2007).
[37] See the Supplemental Material http://link.aps.org/supplemental/10.1103/PhysRevLett.116.106101, which includes Refs. [39–43], for additional theoretical and experimental details related to the $BaTiO_3$/Ge interfacial structure.
[38] J. P. Perdew, K. Burke, and M. Ernzerhof, Generalized gradient approximation made simple, Phys. Rev. Lett. **77**, 3865 (1996).
[39] D. Vanderbilt, Soft self-consistent pseudopotentials in a generalized eigenvalue formalism, Phys. Rev. B **41**, 7892 (1990).
[40] N. Marzari and D. Vanderbilt, Maximally localized generalized Wannier functions for composite energy bands, Phys. Rev. B **56**, 12847 (1997).
[41] P. Giannozzi, S. Baroni, N. Bonini, M. Calandra, R. Car, C. Cavazzoni, D. Ceresoli, G. L. Chiarotti, M. Cococcioni, and I. Dabo, QUANTUM ESPRESSO: a modular and open-source software project for quantum simulations of materials, J. Phys. Condens. Matter **21**, 395502 (2009).
[42] L. Bengtsson, Dipole correction for surface supercell calculations, Phys. Rev. B **59**, 12301 (1999).
[43] A. M. Kolpak and S. Ismail-Beigi, Lattice dynamics of $BaTiO_3$, $PbTiO_3$, and $PbZrO_3$: A comparative first-principles study, Phys. Rev. B **85**, 195318 (2012).
[44] P. Ghosez, E. Cockayne, U. Waghmare, and K. Rabe, Lattice dynamics of $BaTiO_3$, $PbTiO_3$, and $PbZrO_3$: A comparative first-principles study, Phys. Rev. B **60**, 836 (1999).
[45] S. Baroni, S. de Gironcoli, A. D. Corso, and P. Giannozzi, Phonons and related crystal properties from density-functional perturbation theory, Rev. Mod. Phys. **73**, 515 (2001).
[46] W. Zhong, D. Vanderbilt, and K. M. Rabe, Phase Transitions in $BaTiO_3$ from First Principles, Phys. Rev. Lett. **73**, 1861 (1994).
[47] G. Henkelman, B. P. Uberuaga, and H. Jónsson, A climbing image nudged elastic band method for finding saddle points and minimum energy paths, J. Chem. Phys. **113**, 9901 (2000).